

Article

Study of Green Synthesis of Ultrasmall Gold Nanoparticles Using *Citrus Sinensis* Peel

Bo Yang^{1,2,*}, Feng Qi³ , Jingwen Tan³, Tao Yu¹ and Chengtun Qu²

¹ Shaanxi Oil and Gas Pollution Control and Reservoir Protection Key Laboratory, Xi'an Shiyou University, Xi'an 710065, Shaanxi, China; 180708@xsyu.edu.cn

² State Key Laboratory of Petroleum and Petrochemical Pollution Control and Treatment, Beijing 102206, China; xianqct@xsyu.edu.cn

³ Department of Mechanical and Aerospace Engineering, University of Missouri-Columbia, Columbia, MO 65211, USA; gielcheen@gmail.com (F.Q.); jt7k4@mail.missouri.edu (J.T.)

* Correspondence: yangbo@xsyu.edu.cn; Tel.: +86-1860-290-4820

Received: 8 May 2019; Accepted: 3 June 2019; Published: 14 June 2019



Abstract: Sweet orange (*Citrus sinensis*) peel, one of the most underutilized biowaste, was in this study employed for the green synthesis of gold nanoparticles (AuNPs) as an alternative source of reductant and stabilizer. Spherical AuNPs with narrow size distribution (1.75 ± 0.86 nm) were obtained by controlling pH and adjusting sequence for the first time. ultraviolet-visible (UV-vis) spectrophotometer, transmission electron microscopy (TEM), energy-dispersive spectroscopy (EDS), dynamic light scattering (DLS) were applied to detect the characteristic surface plasmon resonance peak, morphological and aggregate characteristic, elementary composition and hydrodynamic diameter, respectively. The major functional groups in extract were tested by Fourier transform infrared (FT-IR) spectrophotometer to characterize the components which are responsible for the reduction and stabilization of AuNPs. The possible role of the components during the process of AuNPs synthesis is also discussed. The result of this study enriched the green source for ultra-small AuNPs synthesis, and will help to understand the mechanism of synthesis and stability of ultra-small AuNPs by fruit peels extract.

Keywords: biowaste; green synthesis; gold nanoparticles; functional groups; mechanism

1. Introduction

Nanotechnology is one of the most important technologies in all areas of science due to the significant difference in nature properties of nanoparticles [1–4], and these properties (e.g., biological, catalytic activity, mechanical properties, melting point optical absorption, thermal and electrical conductivity) are dominated by their size, shape and distribution [5,6]. Traditionally, nanoparticles could be produced and stabilized by two different ways. The physical methods are based mostly on the energy transfer that occurs in an irradiated material by ionizing or non-ionizing radiation, leading to the generation of reducing agents responsible for the nucleation of metallic particles. These methods include radiation [6] and laser ablation [7], among others. Most of the physical methods are green approaches, however, because of the radiation dose control and the lack of stabilizers, the production of stable gold nanoparticles (AuNPs, ≤ 2 nm) with narrow distribution by physical methods are rarely reported [6]. The chemical methods are a redox reaction between material and reducing agents such as sodium borohydride [8], hydrazine [9], and triethyl amine [10]. These are currently the most explored pathways for the synthesis of gold nanoparticles due to their ease of performance, high production yield and stability, despite that they are known to be biologically and environmentally toxic. Metallic nanoparticles of noble metals such as gold, silver, platinum, and palladium have been

widely used in products ranging from cosmetic to medical and pharmaceuticals. AuNPs, noble metal nanoparticles that are characterized by stability, less toxicity, and biocompatibility, are widely used in biological systems for various novel applications [11,12]. AuNPs could be synthesized by physical and chemical approaches, however in order to produce AuNPs with size less than 5 nm, chemical reductants and protecting agents commonly are used for the particles size tuning and stabilizing, which are often toxic and hard to remove from the AuNPs suspension [13–15]. These AuNPs synthesized by chemical agents often lead to inconsistent toxicity risks in biological tests [16–21]. Therefore, developing an environmental friendly method that is toxic chemicals free is crucial, especially in medical and pharmaceutical areas.

In our previous research, uniform small to ultra-small AuNPs with controllable size and high stability were synthesized successfully via green synthesis (using fruit juices/extracts) [22]. However, the major functional groups that are responsible for the reduction of AuNPs, the possible role in the synthesis and stabilization of ultra-small AuNPs, are still unknown. As a foodstuff source, fruit juices/extracts are not the best choice for the green synthesis at industrial-scale production, based on economic reasons.

Since green synthesis is a method that uses natural products (such as plants, enzymes, fungi and algae) as both reductant and stabilizer, it is possible to find an alternative natural product source such as peel, stem and leaf to instead of fruits [23–26].

Citrus peels is one of the most underutilized and geographically diverse biowaste residues. At present, the worldwide industrial citrus wastes account for 50 wt% of the original whole fruit mass, and almost 1/2 of the citrus wastes is peel [27–29]. The management of these wastes that produce odor and soil pollution still remains a major problem in the food industry [30]. At present, there are many researches related to the green synthesis of AuNPs by orange peel were conducted, however, the particles produced by those researches are usually bigger than 5 nm [2,31,32].

Thus, in this study, extract from biowaste *Citrus sinensis* (*C. sinensis*) peels was delicately used as a reducing agent to prepare uniform-sized AuNPs by controlling pH and sodium hydroxide adding sequence. As a result, stable AuNPs with ultra-small size (<2 nm) were successfully obtained from freshly prepared *C. sinensis* peel extract for the first time. Based on this method, the mechanism of reduction and dispersion stability of the functional groups was explored.

2. Materials and Methods

2.1. Materials and Reagents

Hydrogen tetrachloraurate-(III) trihydrate (HAuCl_4 , 30 wt%) was purchased from Sigma-Aldrich (St.Louis, MO, USA). Sodium hydroxide (NaOH) was provided from Fisher Scientific (Pittsburgh, PA, USA). Fresh *C. sinensis* were purchased from a Wal-Mart local store Columbia, MO, in USA.

2.2. *C. Sinensis* Peels Extract

Fresh *C. sinensis* peels were washed thoroughly with running water to remove dirt, and washed again with distilled water. 200 g cleaned and dried (by filter paper) *C. sinensis* peels were cut into small pieces (about 9 mm^3) and immersed in 400 mL deionized water at $60 \text{ }^\circ\text{C}$ for 30 min [1]. After being cooled down to room temperature, the peels-immersion water was filtered (by filter paper, No.5 Whatmen, Fisher Scientific), centrifuged (12000 rpm for 5 min) and collected for further testing in 24 h.

2.3. Synthesis of AuNPs Using Fresh *C. sinensis* Peel Extract

0.75 mL of HAuCl_4 solution (2.00 mM) was mixed with 2.05 mL deionized water and preheated to $100 \text{ }^\circ\text{C}$ in water bath. Then, 0.20 mL of fresh *C. sinensis* peel extract (preheated to $100 \text{ }^\circ\text{C}$) was added into the solution. After the reaction began (solution colour changed from golden to red), the mixture solution was continuously heated for 5 min in $100 \text{ }^\circ\text{C}$ water bath to make sure Au^{3+} fully consumed. Three parallel samples were made for each *C. sinensis* peel extract.

2.4. Effect of pH on AuNPs Size Distribution and Morphology

Different volumes of 0.2 M NaOH (0, 30, 40, 60, and 100 μL) solution were added into mixture solutions (see Section 2.3) to control the pH to 3 (control), 6, 8, 10, and 11, respectively. In order to keep the volume of solutions constant at 3.0 mL, volumes of deionized water in mixture solutions were decreased from 2.05 to 2.02, 2.01, 1.99 and 1.95 mL, correspondingly. Afterwards, the solutions were heated in a water bath (100 $^{\circ}\text{C}$), added to 0.20 mL of the preheated (100 $^{\circ}\text{C}$) fresh *C. sinensis* peel extract, then waited for 5 min after the reaction started. The AuNPs in different pH conditions were synthesized by the same process in triplicates.

2.5. Analysis and Characterization of AuNPs by UV-vis, EDS, TEM, DLS, FT-IR

UV-visible (UV-vis) absorption spectra of the AuNPs solutions were recorded in the wavelength range of 400–750 nm on a double beam Shimadzu UV-vis spectrophotometer. The elemental analysis of AuNPs was processed by a scanning electron microscope (SEM) (JEOLJSM-6360A, (Columbia, MO, USA) equipped with energy-dispersive spectrometer (EDS). JEOLJEM-1400 120 kV TEM (JEOL, Columbia, MO, USA) was used for taking TEM images of the AuNPs.

The TEM samples preparation and images acquisition principle are all followed by our previous study [22]. Briefly, 5.0 μL of the AuNPs solution droplet was deposited onto carbon-coated copper grids, and the excess solution was wiped away with a filter paper (see Section 2.2) after 30 min. Then, the copper grids were dried in air for 10 min. In order to guarantee enough images that could represent a significant statistical amount of the tested AuNPs, 10 TEM images with the same magnification were taken for each sample batch. The hydrodynamic diameters were measured by DLS, using a Zetasizer Nano (Malvern Panalytical, Malvern, UK). FT-IR measurement was carried out using Cary 660, FT-IR spectrophotometer by employing KBr pellet technique. The FT-IR spectra were collected from 32 scans at a resolution of 4 cm^{-1} in the transmission mode (4000–400 cm^{-1}).

2.6. Aging and 72 h-Incubation Test

The AuNPs solution was placed in glass bottle and sealed, after four months stored at room temperature, the morphology and dispersion of the AuNPs solution were examined by TEM. At room temperature, 9 mL sodium chloride solution (1 mM) and 1 mL AuNPs solution were added to form gold nanoparticles salt solution. The AuNPs salt solution was placed in room temperature for 72 h, and the AuNPs were characterized again for their stability by TEM.

2.7. Image Processing

Based on TEM images, the average nanoparticles size and their size distribution were analyzed by ImageJ1.50i [24]. Ten TEM images, containing at least 100 particles in each of the images, were applied to calculate the sizes of AuNPs, including their statistically significant mean and standard deviation values.

3. Results and Discussion

3.1. Formation of AuNPs Using Fresh *C. sinensis* Peel Extract at Different pHs

In this study, we aimed to investigate the pH effect on the production of AuNPs when pHs (from 6 to 11) adjusted before the reaction started. We were particularly interested in investigating the appearance characteristics (such as shape, size, etc.) and distribution of the formed AuNPs. The AuNPs which synthesized at different pHs were analyzed using an UV-vis spectrophotometer. The absorbance curves of the AuNPs obtained are shown in Figure 1. The maximum absorption wavelength ($\lambda_{\text{max}} = 545 \text{ nm}$) in Figure 1 is found in the control group (pH = 3), and shifts from 536 nm to 529 nm (blue shift) along with the solution pH increases from 3 to 11. It means that increasing the pH of a solution decreases the AuNPs size. Additionally, inverse correlation between the absorbance intensity

of AuNPs and the solution pH occurs. The absorbance intensity of all the AuNPs groups decreases, accompanied by the increase in pH (pH = 6, 8 and 11). Compared to the absorbance intensity of 1.33 at $\lambda_{\max} = 545 \text{ nm}$ (control), only 0.67 is observed at $\lambda_{\max} = 536 \text{ nm}$ when pH is 8.

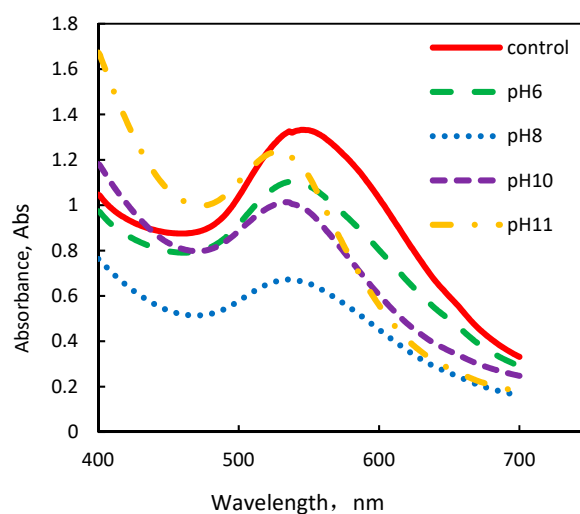


Figure 1. UV-vis spectra of AuNPs solutions obtained from *Citrus sinensis* (*C. sinensis*) peel at different pHs adjusted before the reaction.

3.2. Elements Contained Analysis of AuNPs by EDS

Energy-dispersive spectroscopy (EDS) analysis was performed to detect the elements contained in AuNPs solution when pH = 11. As shown in Figure 2, a strong signal is observed around 2.2 keV, which confirms the existence of Au in the solution where the redox reaction happened between Au^{3+} and the fruit peel extract. Meanwhile, C, O, and Na elements are observed on the fabricated AuNPs EDS spectra. These elements exist in the cellulose and salinity in *C. sinensis* peel extract. NaOH solution is the other source of Na atoms.

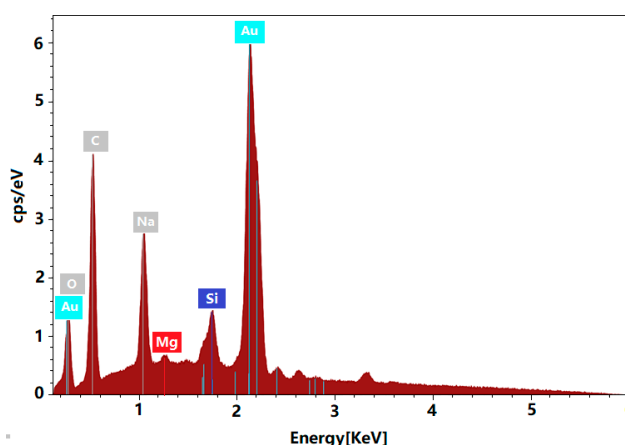


Figure 2. Energy-dispersive spectroscopy (EDS) spectra of the fabricated AuNPs obtained from *C. sinensis* peel at pH = 11.

3.3. Morphology Analysis of AuNPs by TEM

In order to investigate the appearance characteristics of AuNPs, TEM was used to characterize the sample AuNPs colloidal solutions formed in *C. sinensis* peel extract at different pHs. Figure 3 presents the TEM images of AuNPs formed in *C. sinensis* peel extract at pH of 3, 6, 8, 10, and 11, respectively. Spherical AuNPs particles are observed in all of the prepared solutions, while the AuNPs sizes decreased with increase in pH of solution. The particles sizes in different pHs were evaluated by

ImageJ software. The sizes of AuNPs obtained from *C. sinensis* peel extract at different experimental conditions are listed in Table 1. It was found that along with the NaOH increase in solution, the images of AuNPs (Figure 3a–e) show a considerable improvement on size distribution and shape of the AuNPs. The measured AuNPs sizes were reduced significantly, when pH increased from 3 (control) to 11. Our previous result has proved, in consistency with others, that the increase in pH has a negative effect on the particle quantity [6,22,25,33]. It means fruit peel extracts have a similar effect on synthesis of AuNPs with fruit juices/ extracts, and could be an alternative source for synthesis of ultra-small AuNPs.

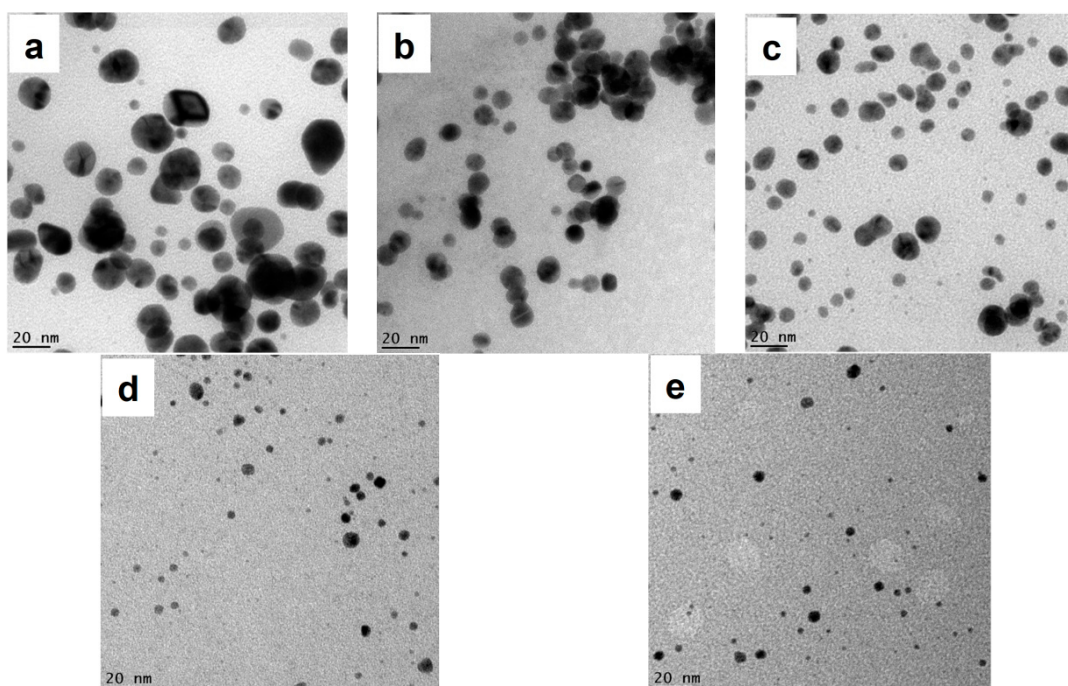


Figure 3. TEM images of AuNPs formed in *C. sinensis* peel extract at different pHs adjusted before the reaction: (a) pH = 3 (control); (b) pH = 6; (c) pH = 8; (d) pH = 10; (e) pH = 11.

3.4. Tuning AuNPs Size and Size Distribution

Similar with foodstuff sources (juice/extracts) [22], the morphology and size of the synthesized AuNPs by biowaste (*C. sinensis* peel extract) were influenced by NaOH in solutions. In the present study, the synthesized particles in the high pH solution showed a reduction of particle sizes. Meanwhile, these particles possessed a narrower size distribution in a spherical shape. However, limited quantity of Au nanoparticles was synthesized using high pH solution. Very few free Au^{3+} ions could participate in the AuNPs generation reaction, since the reaction of Au^{3+} and OH^- ($\text{Au}^{3+} + \text{OH}^- = \text{Au}(\text{OH})_3$) occurred first, and the reduced absorbance in UV-vis spectra was observed as a result. In order to restrict the particle size growth and increase the quantity of AuNPs, most Au^{3+} ions are ought to receive electrons from the functional groups of *C. sinensis* peel extract instead of hydroxyl ions in solution.

To avoid $\text{Au}(\text{OH})_3$ formation, the order of adding hydroxyl ions solution was changed according to our former result, specifically [22]. First, the *C. sinensis* peel extract was added into and mixed with excess Au^{3+} ions solution. Then, the hydroxyl ions were added into the prepared reaction mixture. Hence, Au^{3+} ions are possible to react with the functional groups in the *C. sinensis* peel extract to produce AuNPs during the early stage of reactions instead of $\text{Au}(\text{OH})_3$ generation. Then, pH of the solution was increased to impose restriction on the further growth of nanoparticles by starting reaction of Au^{3+} and OH^- . When compared to the former protocol (adding hydroxyl ions before reaction), the amount of hydroxyl ions, gold ions and peels extract were constant. However, the intervention time of hydroxyl ions on the reaction was different. As shown in Figure 4, all maximum absorbance for each curves are higher than those of the method that pH was adjusted before the reaction (see

Table 1), which indicates that more Au³⁺ ions are reduced to AuNPs instead of Au(OH)₃ by reacting with hydroxyl ions. Moreover, the present of lower λ_{max} = 522 (compare to λ_{max} = 529 when pH = 11 adjust before reaction) demonstrates that even smaller (compare to fruit extract source) AuNPs (<2 nm) are formed during this reaction sequence.

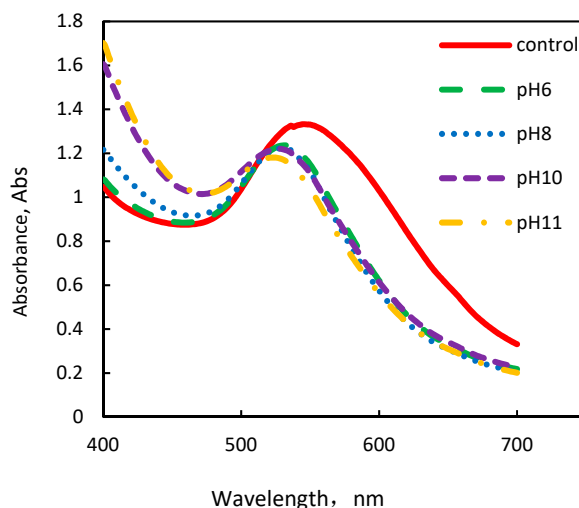


Figure 4. UV-vis spectra of AuNPs solutions obtained from *C. sinensis* peel at different pHs adjusted after the reaction.

Table 1. Summary of the peak wavelength (λ_{max}), intensity, and size of AuNPs obtained from *C. sinensis* peel at different experiment condition.

| | Size (nm) | Absorbance | λ _{max} (nm) | Size(nm) | Absorbance | λ _{max} (nm) |
|---------|--------------------------------|------------|-----------------------|-------------------------------|------------|-----------------------|
| Control | 12.32 ± 4.56 | 1.33 | 546 | 12.32 ± 4.56 | 1.33 | 546 |
| | Adjust pH before Reaction (nm) | | | Adjust pH after Reaction (nm) | | |
| pH 6 | 9.33 ± 2.37 | 1.10 | 536 | 4.91 ± 3.03 | 1.24 | 531 |
| pH 8 | 7.15 ± 3.38 | 0.67 | 536 | 6.33 ± 2.56 | 1.22 | 530 |
| pH 10 | 3.07 ± 1.69 | 1.01 | 534 | 1.99 ± 0.84 | 1.22 | 526 |
| pH 11 | 2.79 ± 1.53 | 1.24 | 529 | 1.75 ± 0.86 | 1.18 | 522 |

Figure 5 illustrates the TEM images of nanoparticles synthesized using the *C. sinensis* peel extract at different pHs which are adjusted after the reaction. It could be observed from the images that the size distribution of particles is much narrower than those in Figure 3 which were prepared by the method of pH adjustment before reaction, and most of the particles are spherical. Furthermore, the nanoparticles sizes are decreased to smaller than 5 nm (4.91 ± 3.03 nm, Figure 5a) from 9.33 ± 2.37 (Figure 3b) with the new pH adjusting sequence. The number of large particles is limited (Figure 5c,d) compare to Figure 3d,e. For *C. sinensis* peel extract with the new pH adjusting method (adjust after reaction happened), all the AuNPs sizes are restricted to smaller than 2 nm (see Table 2) with good dispersity when the pH was 11 (Figure 5d). Furthermore, no aggregation of AuNPs was found at such experimental condition. The results of the study indicate that hydroxyl ions could be used to tune the sizes and size distributions of AuNPs by choosing different NaOH adding opportunity windows. Optimal dosage of hydroxyl ions can restrict further growth of small nanoparticles and optimize size distribution.

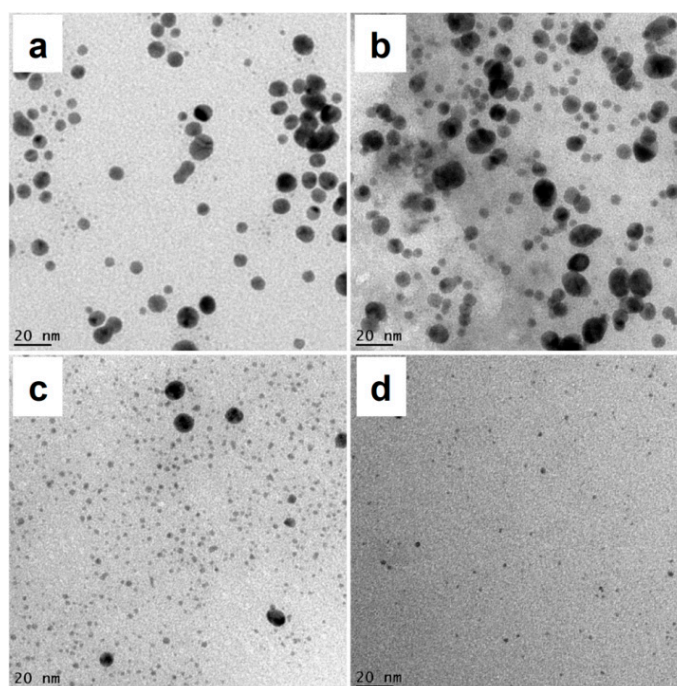


Figure 5. (a–d) Illustrates the transmission electron microscopy (TEM) images of nanoparticles synthesized using the *C. sinensis* peel extract at different pHs which are adjusted after the reaction.

Table 2. Summary of the peak wavelength (λ_{\max}), Intensity, size of AuNPs obtained from *C. sinensis* peel at different experiment conditions.

| Bond | Type of Vibration | Control Spectrum (cm ⁻¹) | Adjust pH before Reaction (cm ⁻¹) | Adjust pH after Reaction (cm ⁻¹) |
|-----------------|------------------------------------|--------------------------------------|---|--|
| O-H | Alcohol, phenols, Carboxylic acids | 3363 | 3434 | 3436 |
| N-H | Amines | | | |
| C-H | Alkanes | 2929 | 2969, 2944 | 2931 |
| C=O | Carboxylic acid or Ester | 1724 | 1737 | 1724 |
| N-C=O | Amide I bond of proteins | 1608 | 1635 | 1631 |
| CH ₂ | Alkanes | 1367 | 1363 | 1346 |
| C-O | Carboxylic acid, ester, or ether | 1203 | 1216 | 1203 |
| C-N | Aliphatic amines or alcohol/phenol | 1058 | 1070 | 1058 |

3.5. Hydrodynamic Diameter Analysis of AuNPs by DLS

The DLS measurement demonstrates (Figure 6) that the average size of the AuNPs formed from the *C. sinensis* peel at pH = 11 adjusted after the reaction in colloidal solution was 2.11 ± 1.01 nm (1.75 ± 0.86 by ImageJ). The reasons for the difference in size distribution between DLS and ImageJ software based on TEM are as follow: (1) DLS measures the hydrodynamic size rather than the bare particle as in TEM; (2) the plant extracts used in this study contain a large number of plant fibers, protein and other substance, which will surround or adhere to the surface of the particles during the formation of AuNPs, resulting in larger DLS size than TEM size; (3) metal crystals have completely different colors from organic matter in TEM images, the biological material on the AuNPs surface disturbs the DLS measurement which could be ignored during manual label the particles size before measurement by ImageJ software. Based on these results, the nanoparticles sizes were evaluated by ImageJ software in this study.

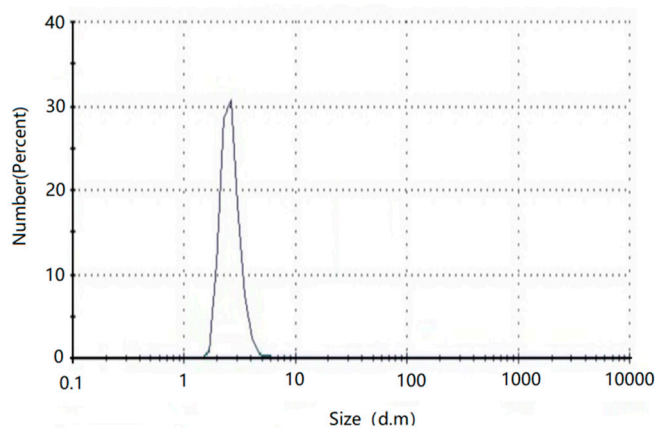


Figure 6. Hydrodynamic diameter measurement of AuNPs formed from *C. sinensis* peel at pH = 11 adjusted after the reaction.

3.6. FT-IR Analysis of AuNPs

FTIR was carried out to determine the major functional groups that are responsible for the reduction of Au^{3+} in solution. Besides, the possible mechanism in the synthesis and stabilization of the ultra-small sized AuNPs that were obtained by adding OH^- into peel extract in different sequences is discussed. Figure 7 illustrates the FT-IR spectra obtained from control group (curve a: Au^{3+} and *C. sinensis* peel extract mixed solution, nothing reacting with Au^{3+}), the pH adjusted to 11 before synthesis reaction (curve b) and pH adjusted to 11 after AuNPs synthesis reaction (curve c).

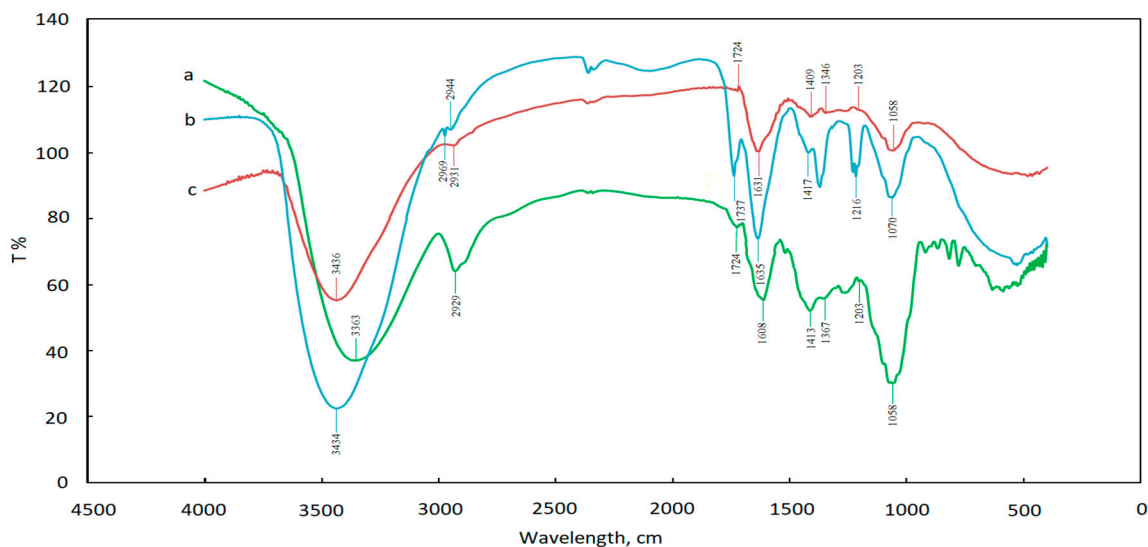


Figure 7. The FT-IR spectra of AuNPs solution obtained from *C. sinensis* peel extract at different experiment conditions: (a) control; (b) pH adjust to 11 before AuPNs synthesise reaction happen; (c) pH adjust to 11 after AuPNs synthesise reaction happen.

The curve a shows several peaks indicating the complex nature of the biological material. The bands appearing at 3363, 2929, 1724, 1608, 1367, 1203 and 1070 cm^{-1} are assigned to stretching vibration of O-H of alcohol or N-H of amines, C-H of alkanes, C=O of carboxylic acid or ester, N-C=O amide I bond of proteins, CH_2 of alkanes, C-O of carboxylic acid, ester, or ether, and C-N of aliphatic amines or alcohol/phenol, respectively [34]. After reaction with HAuCl_4 , the shift of the peaks for both two different pH adjusting sequences (curve b and c) indicates that the carboxyl, hydroxyl and amide groups in *C. sinensis* peel extract may participate in the nanoparticles synthesis (see Table 2). It also shows that the major stretching appearing at 3000–3500 cm^{-1} indicates the presence of O-H stretch

due to the presence of pheols, flavonoids, benzophenones and anthocyanins [35]. A different shifting occurs here, indicating that different amount of carbonyl groups in the *C. sinensis* peel extract were taken part into the redox reaction (see Section 3.4). A bigger shifting could be observed on curve c (3436 cm^{-1}) than curve b (3434 cm^{-1}) suggesting that more AuNPs were occurred and more carbonyl groups were participated in the reaction when pH adjusted after reaction starting, than the reaction when pH adjusted before reaction starting. Thus, the results (the reaction $\text{Au}^{3+} + \text{OH}^- = \text{Au}(\text{OH})_3$ would decrease the generation of AuNPs and stop the growth of AuNPs size) obtained in Section 3.4 was verified.

Aside the O-H stretching, the region of 2929 cm^{-1} presents the C-H in xanthone [36]. Bands of C-H bond from *C. sinensis* peels extract were split into two; 2944 cm^{-1} and 2969 cm^{-1} (curve b). No peak split is observed after the pH adjusting (curve c). These results suggest that, after the generation of AuNPs, the transmittance changed. Meanwhile, with the generation of AuNPs, the C=O stretching characteristic peak at region of 1700 cm^{-1} is observed, and the peak in curve b shifts to red (1737 cm^{-1}), compared to the peaks in curve a and c (1724 cm^{-1}), which means that the consumption of carbonyl substance might be related to pH increase. The reasons for the speculation above are as follows: (1) for solution of curve a and c, they have the same properties before the reaction happened; (2) for solution of curve b, *C. sinensis* peels extract were added into a high pH solution; (3) for solution of curve c, the extracts were added into the solution before pH adjusted, and part of -OH were reacted with Au^{3+} to product $\text{Au}(\text{OH})_3$ instead of effecting carbonyl substance existence in solution. The combination of this peak shift phenomenon with TEM images (Figures 3e and 5d) indicates that the existence of carbonyl substances help the size of the AuNPs stabilization [37]. Besides, C-O stretch can be found in the range of $1300\text{--}1000\text{ cm}^{-1}$. The peaks in curve b at 1216 cm^{-1} and 1070 cm^{-1} different from the curve a and c suggest the transmission of C-O bond after AuNPs generation, when the pH is adjusted before reaction starting. It demonstrates that the carboxylic acid and ester in the *C. sinensis* peel extract are consumed in the strongly basic solution, and could protect AuNPs from aggregation before the pH is adjusted to 11.

3.7. Stability of AuNPs at Room Temperature

The dispersion stability of the particles obtained in this research was tested by four-month aging testing at room temperature and 72 h-incubation in 1 mM NaCl (Natural saline) at room temperature [38,39]. Their appearance characteristics were examined by TEM. It could be observed that all the AuNPs showed constant size from two different dispersion stability tests (1.80 ± 0.89 and $1.75 \pm 0.86\text{ nm}$), without any aggregation. TEM results indicate that the AuNPs synthesized in this research are highly stable at room temperature and natural saline, which means they will remain stable when used for biological and medical applications

4. Conclusions

In this study, a green synthesis method with *C. sinensis* peel extract was used to synthesize AuNPs by two different synthesis routes following the previous research. The results indicated that the AuNPs, with better morphological features than those produced from fruit juices/extracts, could be synthesized from fruit waste (*C. sinensis* peel) extract ultra-small AuNPs ($1.75 \pm 0.86\text{ nm}$) were first synthesized by biowaste (*C. sinensis* peel), which is smaller than those ($2.6 \pm 1.1\text{ nm}$) obtained from fruit extract (*M. acuminata*) in our previous experiment. More importantly, the major functional groups that are responsible for the production of the AuNPs, as well as the possible mechanism of the synthesis and stabilization, were investigated by FTIR spectra. Above all, carboxyl, hydroxyl and amide groups in *C. sinensis* peel extract may participate in the process of nanoparticle synthesis, and carbonyl groups helped to stabilize the size of AuNPs. Carboxylic acid and ester in the *C. sinensis* peel extract could protect AuNPs from aggregation before pH is adjusted to 11 and will be consumed in strongly basic solution.

Author Contributions: Conceptualization, B.Y. and C.Q.; methodology, B.Y.; software, J.T.; investigation and data analysis, B.Y. and J.T.; resources, J.T. and F.Q.; data curation, T.Y.; writing—original draft preparation, J.T. and B.Y.; writing—review and editing, B.Y. and F.Q.; supervision, C.Q.

Funding: This research was funded by the Key Laboratory Scientific Research Program of Shaanxi Provincial Education Department, grant number 14JS085, and was supported by the National Science and Technology Major Project of China, grant number 2016ZX05040-003.

Acknowledgments: The authors acknowledge the technical support from Tommi A. White, Martin schauflinger, DeAna Grant and Xiaoqing He, Electron Microscopy Core, University of Missouri.

Conflicts of Interest: The authors declare no conflict of interest.

References

1. Lee, K.X.; Shameli, K.; Miyake, M.; Kuwano, N.; Bt Ahmad Khairudin, N.B.; Bt Mohamad, S.E.; Yew, Y.P. Green synthesis of gold nanoparticles using aqueous extract of garcinia mangostana fruit peels. *J. Nanomater.* **2016**, *2016*, 8489094. [[CrossRef](#)]
2. Islam, N.U.; Ahsan, F.; Khan, I.; Shah, M.R.; Shahid, M.; Khan, M.A. Green synthesis and biological activities of gold nanoparticles functionalized with Citrus reticulata, Citrus aurantium, Citrus sinensis and Citrus grandis. *J. Chem. Soc. Pak.* **2015**, *37*, 721–731.
3. Chow, E. *Gold Nanoparticles: Properties, Characterization and Fabrication*; NOVA Science Publishers Inc.: New York, NY, USA, 2015.
4. Trang, H.D.N.; Vardhanabhuti, B.; Lin, M.S.; Mustapha, A. Antibacterial properties of selenium nanoparticles and their toxicity to Caco-2 cells. *Food Control* **2017**, *77*, 17–24.
5. Daniel, M.C.; Astruc, D. Gold nanoparticles: Assembly, supramolecular chemistry, quantum-size-related properties, and applications toward biology, catalysis, and nanotechnology. *Chem. Rev.* **2004**, *104*, 293–346. [[CrossRef](#)] [[PubMed](#)]
6. Freitas de Freitas, L.; Varca, G.H.C.; Dos Santos Batista, J.G.; Benevolo Lugao, A. An Overview of the Synthesis of Gold Nanoparticles Using Radiation Technologies. *Nanomaterials* **2018**, *8*, 939. [[CrossRef](#)] [[PubMed](#)]
7. Veiko, V.P.; Tyurnina, A.E.; Shur, V.Y.; Kozin, R.V.; Kuznetsov, D.K.; Mingaliev, E.A.; Vartanyan, T.A. Synthesis of stable silver colloids by laser ablation in water. *Int. Soc. Opt. Photonics* **2013**, *9065*, 90650D.
8. Brust, M.; Walker, M.; Bethell, D.; Schiffrin, D.J.; Whyman, R. Synthesis of thiol-derivatised gold nanoparticles in a two-phase liquid–liquid system. *J. Chem. Soc. Chem. Commun.* **1994**, *7*, 801–802. [[CrossRef](#)]
9. Turner, M.; Golovko, V.B.; Vaughan, O.P.H.; Abdulkin, P.; Berenguer-Murcia, A.; Tikhov, M.S.; Johnson, B.F.G.; Lambert, R.M. Selective oxidation with dioxygen by gold nanoparticle catalysts derived from 55-atom clusters. *Nature* **2008**, *454*, 981–983. [[CrossRef](#)] [[PubMed](#)]
10. Mandal, T.K.; Fleming, M.S.; Walt, D.R. Preparation of polymer coated gold nanoparticles by surface-confined living radical polymerization at ambient temperature. *Nano Lett.* **2002**, *2*, 3–7. [[CrossRef](#)]
11. Browning, L.M.; Lee, K.J.; Huang, T.; Nallathamby, P.D.; Lowman, J.E.; Xu, X.H.N. Random walk of single gold nanoparticles in zebrafish embryos leading to stochastic toxic effects on embryonic developments. *Nanoscale* **2009**, *1*, 138–152. [[CrossRef](#)]
12. Leifert, A.; Pan-Bartnek, Y.; Simon, U.; Jahnke-Dechent, W. Molecularly stabilised ultrasmall gold nanoparticles: Synthesis, characterization and bioactivity. *Nanoscale Res. Lett.* **2013**, *5*, 6224–6242. [[CrossRef](#)] [[PubMed](#)]
13. Deraedt, C.; Salmon, L.; Gatard, S.; Ciganda, R.; Hernandez, R.; Didier, J.R.; Astruc, D. Sodium borohydride stabilizes very active gold nanoparticle catalysts. *Chem. Commun.* **2014**, *50*, 14194–14196. [[CrossRef](#)] [[PubMed](#)]
14. Tajammul Hussain, S.; Iqbal, M.; Mazhar, M. Size control synthesis of starch capped-gold nanoparticles. *J. Nanopart. Res.* **2009**, *11*, 1383–1391. [[CrossRef](#)]
15. Eustis, S.; Hsu, H.Y.; El-Sayed, M.A. Gold nanoparticle formation from photochemical reduction of Au³⁺ by continuous excitation in colloidal solutions: A proposed molecular mechanism. *J. Phys. Chem. B* **2005**, *109*, 4811–4815. [[CrossRef](#)] [[PubMed](#)]
16. Djafari, J.; McConnell, M.T.; Santos, H.M.; Capelo, J.L.; Bertolo, E.; Harvey, S.C.; Lodeiro, C.; Fernandez-Lodeiro, J. Synthesis of Gold Functionalised Nanoparticles with the Eranthis hyemalis Lectin and Preliminary Toxicological Studies on Caenorhabditis elegans. *Materials* **2018**, *11*, 1363. [[CrossRef](#)] [[PubMed](#)]

17. Shah, M.; Fawcett, D.; Sharma, S.; Tripathy, S.K.; Poinern, G.E.J. Green Synthesis of Metallic Nanoparticles via Biological Entities. *Materials* **2015**, *8*, 7278–7308. [[CrossRef](#)] [[PubMed](#)]
18. Murphy, C.J.; Gole, A.M.; Stone, J.W.; Sisco, P.N.; Alkilany, A.M.; Goldsmith, E.C.; Baxter, S.C. Gold nanoparticles in biology: Beyond toxicity to cellular imaging. *Acc. Chem. Res.* **2008**, *41*, 1721–1730. [[CrossRef](#)] [[PubMed](#)]
19. Connor, E.E.; Mwamuka, J.; Gole, A.; Murphy, C.J.; Wyatt, M.D. Gold nanoparticles are taken up by human cells but do not cause acute cytotoxicity. *Small* **2005**, *1*, 325–327. [[CrossRef](#)] [[PubMed](#)]
20. Pan, Y.; Neuss, S.; Leifert, A.; Fischler, M.; Wen, F.; Simon, U.; Schmid, G.; Brandau, W.; Jahnke-Dechent, W. Size-dependent cytotoxicity of gold nanoparticles. *Small* **2007**, *3*, 1941–1949. [[CrossRef](#)]
21. Ray, P.C.; Yu, H.; Fu, P.P. Toxicity and environmental risks of nanomaterials: Challenges and future needs. *J. Environ. Sci. Health C Environ. Carcinog. Ecotoxicol. Rev.* **2009**, *27*, 1–35. [[CrossRef](#)]
22. Yang, B.; Chou, J.; Dong, X.Q.; Qu, C.T.; Yu, Q.S.; Lee, K.J.; Harvey, N. Size-controlled green synthesis of highly stable and uniform small to ultrasmall gold nanoparticles by controlling reaction steps and pH. *J. Phys. Chem. C* **2017**, *121*, 8961–8967. [[CrossRef](#)]
23. Dauthal, P.; Mukhopadhyay, M. Phyto-synthesis and structural characterization of catalytically active gold nanoparticles biosynthesized using *Delonix regia* leaf extract. *3 Biotech* **2016**, *6*, 118. [[CrossRef](#)] [[PubMed](#)]
24. Chou, J.; Li, X.F.; Yin, Y.F.; Indrisek, N. Determination of antioxidant activities in fruit juices based on rapid colorimetric measurement and characterisation of gold nanoparticles. *Int. J. Environ. Anal. Chem.* **2015**, *95*, 531–541. [[CrossRef](#)]
25. Dhanasekar, N.N.; Rahul, G.R.; Narayanan, K.B.; Raman, G.; Sakthivel, N. Green chemistry approach for the synthesis of gold nanoparticles using the fungus *Alternaria* sp. *J. Microbiol. Biotechnol.* **2015**, *25*, 1129–1135. [[CrossRef](#)] [[PubMed](#)]
26. Khanhzaei, H.; Ahmad, M.B.; Shameli, K.; Ajdari, Z.; Ghani, M.A.; Kalantari, K. Effect of seaweed *Kappaphycus alvarezii* in the synthesis of Cu@Cu₂O core-shell nanoparticles prepared by chemical reduction method. *Res. Chem. Int.* **2015**, *41*, 7363–7376. [[CrossRef](#)]
27. Marín, F.R.; Soler-Rivas, C.; Benavente-García, O.; Castillo, J.; Pérez-Alvarez, J.A. By-products from different citrus processes as a source of customized functional fibres. *Food Chem.* **2007**, *99*, 736–741. [[CrossRef](#)]
28. Braddock, R.J. *Handbook Of Citrus By-Products and Processing Technology*; Wiley: New York, NY, USA, 1999.
29. Balu, A.M.; Budarin, V.; Shuttleworth, P.S.; Pfaltzgraff, L.A.; Waldron, K.; Luque, R.; Clark, J.H. Valorisation of orange peel residues: Waste to biochemicals and nanoporous materials. *ChemSusChem* **2012**, *5*, 1694–1697. [[CrossRef](#)] [[PubMed](#)]
30. Torrado, A.M.; Cortes, S.; Manuel Salgado, J.; Max, B.; Rodriguez, N.; Bibbins, B.P.; Converti, A.; Manuel Dominguez, J. Citric Acid production from orange peel wastes by solid-state fermentation. *Braz. J. Microbiol.* **2011**, *42*, 394–409. [[CrossRef](#)] [[PubMed](#)]
31. Kahrilas, G.A.; Wally, L.M.; Fredrick, S.J.; Hiskey, M.; Prieto, A.L.; Owens, J.E. Microwave-assisted green synthesis of silver nanoparticles using orange peel extract. *ACS Sustain. Chem. Eng.* **2014**, *2*, 367–376. [[CrossRef](#)]
32. Castro, L.; Blázquez, M.L.; González, F.; Muñoz, A.; Ballester, A. Gold, silver and platinum nanoparticles biosynthesized using orange peel extract. *Adv. Mater. Res.* **2013**, *825*, 556–559. [[CrossRef](#)]
33. Singh, P.; Kim, Y.; Zhang, D.; Yang, D. Biological synthesis of nanoparticles from plants and microorganisms. *Trends Biotechnol.* **2016**, *3*, 588–599. [[CrossRef](#)] [[PubMed](#)]
34. Socrates, G. *Infrared Characteristic Group Frequencies*; Wiley-Interscience Publication: New York, NY, USA, 1980.
35. Rao, K.J.; Paria, S. Aegle marmelos leaf extract and plant surfactants mediated green synthesis of Au and Ag nanoparticles by optimizing process parameters using Taguchi method. *ACS Sustain. Chem. Eng.* **2015**, *3*, 438–491. [[CrossRef](#)]
36. Shameli, K.; Ahmad, M.B.; Shabanzadeh, P.; Al-Mulla, E.A.J.; Zamanian, A.; Abdollahi, Y.; Jazayeri, S.D.; Eili, M.; Jalilian, F.A.; Haroun, R.Z. Effect of *Curcuma longa* tuber powder extract on size of silver nanoparticles prepared by green method. *Res. Chem. Int.* **2013**, *40*, 1313–1325. [[CrossRef](#)]
37. Bogireddy, N.K.R.; Anand, K.K.H.; Mandal, B.K. Gold nanoparticles—Synthesis by *sterculia acuminata* extract and its catalytic efficiency in alleviating different organic dyes. *J. Mol. Liq.* **2015**, *211*, 868–875. [[CrossRef](#)]

38. Lee, K.J.; Nallathamby, P.D.; Browning, L.M.; Osgood, C.J.; Xu, X.H.N. In vivo imaging of transport and biocompatibility of single silver nanoparticles in early development of zebrafish embryos. *ACS Nano* **2007**, *1*, 133–143. [[CrossRef](#)] [[PubMed](#)]
39. Lee, K.J.; Browning, L.M.; Nallathamby, P.D.; Osgood, C.J.; Xu, X.H. Silver nanoparticles induce developmental stage-specific embryonic phenotypes in zebrafish. *Nanoscale* **2013**, *5*, 11625–11636. [[CrossRef](#)] [[PubMed](#)]



© 2019 by the authors. Licensee MDPI, Basel, Switzerland. This article is an open access article distributed under the terms and conditions of the Creative Commons Attribution (CC BY) license (<http://creativecommons.org/licenses/by/4.0/>).